Andrzej MATRAS*

SIMULATION AND LABORATORY RESEARCH OF PERMANENT MAGNET DC-MACHINE

SUMMARY

In the paper calculation results of the magnetic field distribution for the DC-machine with permanent magnet is presented. The calculation is performed by finite element method. The results are contained the distributions of magnetic potential and the flux density in the whole regarding area and the mechanical quantity – radial and tangential stress componet. The mentioned calculations are verified by measurements of the flux density distribution in the air-gap at no-load and rated-load state.

***Keywords**: electrical machines, permanent magnets*

BADANIA LABORATORYJNE I SYMULACYJNE MASZYNY PRĄDU STAŁEGO WZBUDZANEJ MAGNESAMI TRWAŁYMI

W artykule przedstawiono wyniki obliczeń rozkładu pola magnetycznego dla maszyny prądu stałego wzbudzanej magnesami trwałymi. Obliczenia zostały wykonane metodą elementów skończonych. Rezultatami są rozkłady potencjału magnetycznego i indukcji magnetycznej w rozpatrywanym obszarze oraz wielkości mechaniczne – składowe normalne i styczne naprężeń. Wspomniane wyniki obliczeń zostały zweryfikowane pomiarami rozkładu indukcji magnetycznej w szczelinie powietrznej w stanie jałowym i przy znamionowym obciążeniu.

***Słowa kluczowe**: maszyny elektryczne, magnesy trwałe*

1. INTRODUCTION

Permanent magnet electrical machines distinguish higher efficiency and reliability, better dynamic parameters and smaller dimensions for a law rated power comparatively to electromagnetic excitation machines [3]. The above advantage and appreciable progress in manufacture of magnetic materials cause, that the machines are more and more frequently used with electrical servo drives for different applications such as aircraft technology, industrial automation and middle level industrial drives [4]. The range of power ratings of the present permanent magnets motors are about 100 kW, but there are also machines of 10 MW [2].

High level dynamic properties of modern electrical drives with permanent magnet electrical machines want to require of more than ten multiplication of the rated current. As a result of it the dynamic processes like start, breaking perform considerably quicker than for traditional machines with the electromagnetic excitation. The operating conditions like these have consequence in the form of requirement about the demagnetizing resistance in the over-current state.

The substantial operating advantage of commutator permanent magnet DC-machine is admissible value of the armature current – several times (up to five) greater than for standard machines, without change for worse of the commutation processes.

Both field and circuit mathematical models are used to describing the permanent magnets electrical machines. The first of them make possible for more synthetic of problem formulation whereas the second afford possibilities for take into account actual magnetic characteristics of a partial fragment of the magnetic circuit, a local level of saturation and magnetic leakage.

2. MATHEMATICAL MODEL

At load, in a permanent magnet DC-machine the waveform of the air-gap magnetic flux density distorts due to the armature reaction. As a result, in certain regions of the permanent magnet the magnetic field strength could have high values and even materials of high coercivity, such as hard ferrites, could be subjected to irreversible demagnetization. Therefore, designing permanent magnet DC-machines, and specially those running at heavy load, a great attention has to be paid to reaction effects.

In order to predict the performances of permanent magnet DC-machines an accurate computation of their magnetic field is essential. The finite element method can be used to calculate the field distribution taking into account the nonlinearity of the materials and the real configuration of the computed domain.

The armature reaction, which appears when a permanent magnet DC-machine is heavy loaded, causes a strongly distortion of the waveform of the air-gap flux density due to the magnetic circuit saturation. In the permanent magnet the armature reaction field increases from the center of the magnet towards the edges and opposes the excitation field at the magnet trailing edge. Between the direction of the magnetic field and the easy magnetizing axis of the permanent magnet will be a certain angle, dependent on saturation. This could be interpreted as a magnetic coupling between the *d* and *q* axes of the machine, and and as a between the

* Katedra Maszyn Elektrycznych, AGH

easy magnetized (preferred) axis and the hard magnetized (traverse) axis, respectively.

The model of permanent magnet is determined with the demagnetizing curve, the value of remanence flux density and the direction of magnetization. The applied model of magnet can be presented as follows

$$\begin{bmatrix} B_\zeta \\ B_\eta \end{bmatrix} = \begin{bmatrix} \mu_0 & 0 \\ 0 & \mu_0 \end{bmatrix} \begin{bmatrix} H_\zeta \\ H_\eta \end{bmatrix} + \begin{bmatrix} M_\zeta \\ 0 \end{bmatrix} \tag{1}$$

where $O\zeta$ is the direction of magnetization

The demagnetizing curve should define nonlinear characteristic in whole range (usually from the point (B_{rem}) to the point (0, H_c) but for large load also the part for $B < 0$).

The finite element equations are obtained by the minimization of the conventional energy functional

$$F = \int_\Omega \left(\int_0^B \nu \mathbf{B} \cdot \mathbf{dB} - \mathbf{J} \cdot \mathbf{A} \right) d\Omega \tag{2}$$

A Newton–Raphson iterative technique could be applied to a local linearize the resulting system of equations.

$$A^{(k+1)} = A^{(k)} - \left[\frac{\partial \left(S^{(k)} A^{(k)} \right)}{\partial A^{(k)}} \right]^{-1} \left(S^{(k)} A^{(k)} - F^{(k)} \right) \tag{3}$$

3. CALCULATION RESULTS

In this paper the field and electromagnetic torque for the permanent magnet commutator DC-machine is performed. For the electromagnetic torque calculating the Maxwell stress tensor method is selected.

The motor used in this simulation has the following rated parameters:

U_a = 24 V,
I_a = 6 A,
P = 120 W,
n = 720 rpm,

and the design data in Table 1.

Table 1. The motor design characteristics

The rotor outside diameter	76.3 mm
The air-gap thickness	0.8 mm
The poles number	4
The armature winding type	simple wave
The rotor slots number	21
The axial rotor core length	83.6 mm
The commutator segments number	41
The axial magnet length	97.3 mm
No skewing of magnets or rotor slots is employed	

The machine under investigation is without auxiliary poles and pole shoes. The ferrite permanent magnet in the machine is radially magnetized. Its demagnetizing characteristic is presented in Figure 1. In the next figure (Fig. 2) the magnetizing characteristic of armature core is shown.

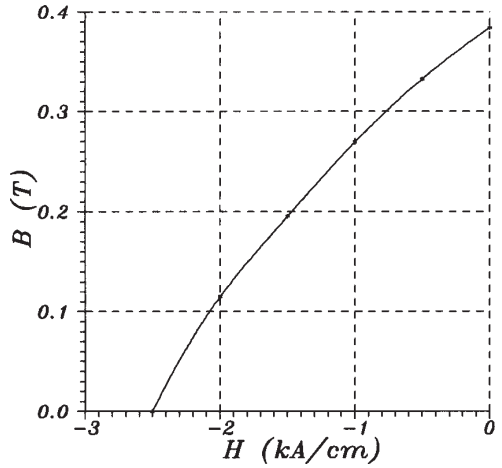

Fig. 1. The demagnetizing characteristic of the permanent magnet

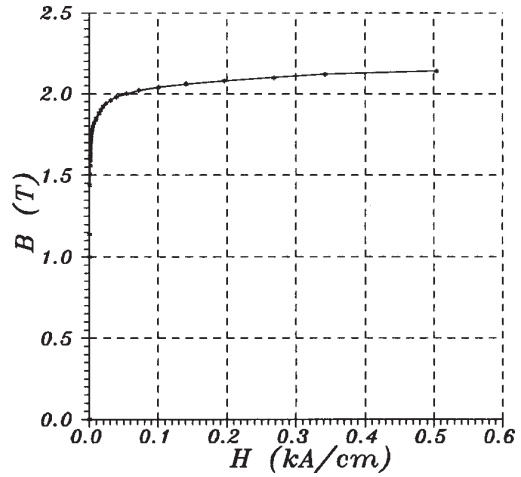

Fig. 2. The magnetizing characteristic of the rotor magnetic circuit

Finite element method is used to determine the flux distribution in the permanent magnet DC-machine.

The following assumption are set:
- machine geometry is reduced to 2-dimensional problem (end effects are neglected),
- due to lack symmetry (number of rotor slots is equal to 21, while number of poles is 4) the whole cross-section of the machine is taken into account,
- the permanent magnet is assumed isotropic but having nonlinear demagnetizing characteristic,
- the magnetizing characteristic of the iron elements are assumed nonlinear, but the hysteresis loop is neglected,
- zero Dirichlet condition is assumed for the outer diameter of the stator core and the shaft.

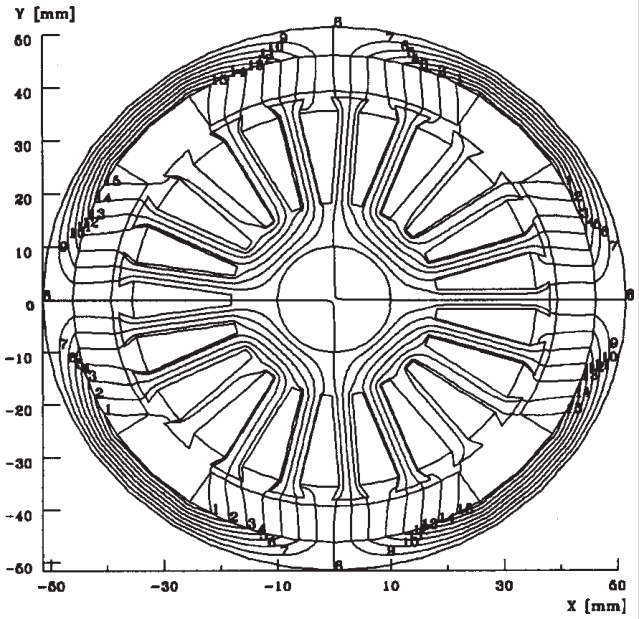

Fig. 3. Field distribution at no-load state

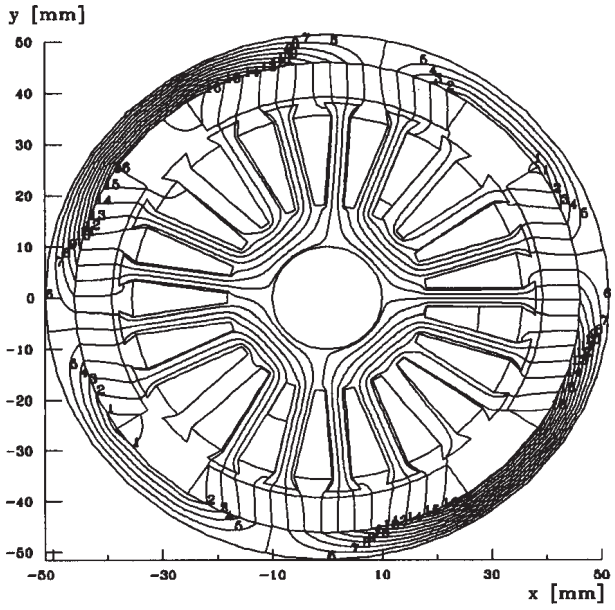

Fig. 4. Field distribution at full load state

Calculations were realized with Vector Fields program Opera-2d.

Calculation results can be divided into three groups:

1) field distribution plots,
2) flux density,
3) the Maxwell stress tensor.

All of these results are both presented the no-load and the rated-load state. Boundary of the rotor teeth and slots and the stator permanent magnets is put on the plots of all quantities depended on φ-angle. It facilitate to connection the presented functions and details of the motor magnetic circuit. In compliance with the Figure 11 these quantities are calculated on the circle of radius

$$r_r + \frac{\delta}{3} \approx 38.42 \text{ mm},$$

where:

r_r – the rotor radius,
δ – the air-gap thickness.

Boundary of the air-gap is put in all figures which presented flux density or stress distribution in this gap. Magnetic field distribution in the whole cross-section of the machine are presented: in Figure 3 for the no-load state case and in Figure 4 for the rated-load state.

In opposite to the first plot, in the Figure 4 distortion of the flux density due to the armature reaction could be observed (as mentioned above the machine have not been auxiliary poles).

In the two next figures radial component of flux density in the air-gap of the machine are plotted. These distributions correspond with the flux plot presented in Figures 3 and 4. Both in the Figure 5 (no-load case) and Figure 6 (full load) calculated results are drawn with solid line while measurements with dotted line.

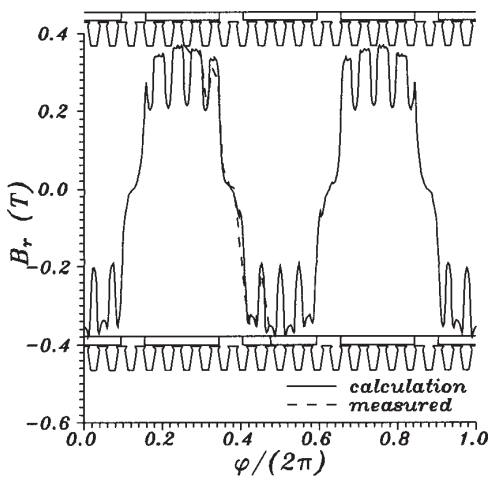

Fig. 5. Flux density *r*-component in the air-gap of the machine at no-load state

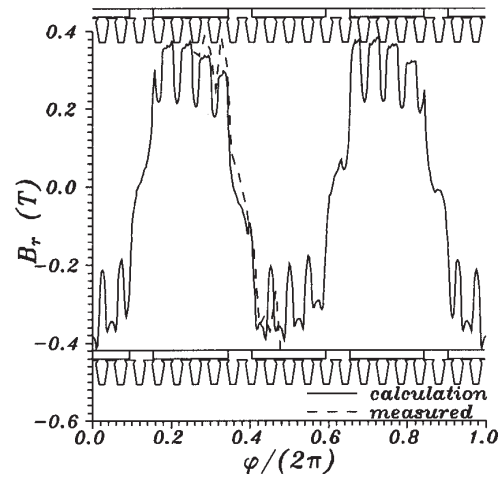

Fig. 6. Flux density *r*-component in the air-gap of the machine at rated-load state

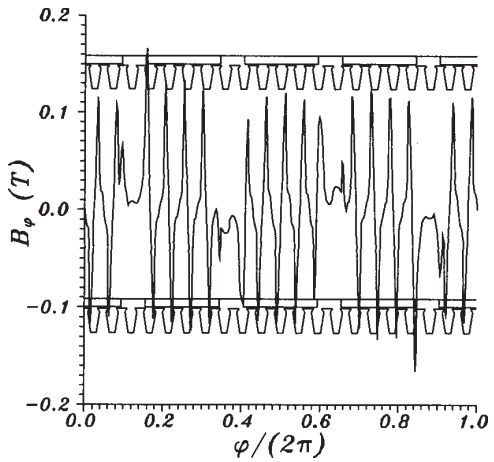

Fig. 7. Flux density φ-component in the air-gap of the machine at no-load state

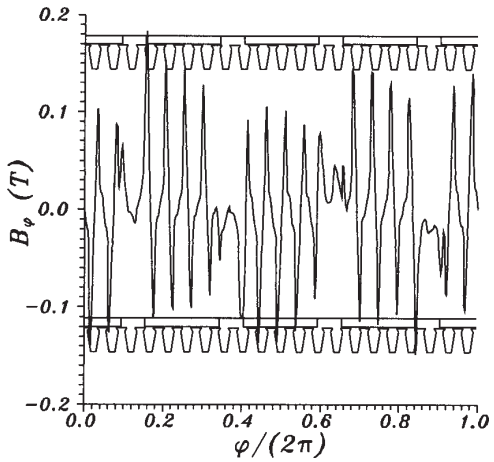

Fig. 8. Flux density φ-component in the air-gap of the machine at rated-load state

Suitable tangential component of this quantity are shown in Figure 7 and 8.

The magnetic flux density is measured with Hall-effect device relocated in the air-gap of the machine. The presented outcomes are carried out with the broken rotor. Small value of the air-gap thickness makes such measurements with the rotation armature completely impossible.

Comparison of calculation and measured value of the flux density *r*-component is better observable in Figures 9 and 10.

The force is calculated using the Maxwell stress tensor on a surface *S*

$$\begin{bmatrix} F_r \\ F_\varphi \end{bmatrix} = \oint_s \begin{bmatrix} T_{rr} & T_{r\varphi} \\ T_{\varphi r} & T_{\varphi\varphi} \end{bmatrix} \begin{bmatrix} \cos(\mathbf{n}, \mathbf{1}_r) & 0 \\ 0 & \cos(\mathbf{n}, \mathbf{1}_\varphi) \end{bmatrix} ds \quad (4)$$

where:

$$T_{rr} = \frac{1}{2}(H_r B_r - H_\varphi B_\varphi) \quad (5)$$

$$T_{\varphi\varphi} = \frac{1}{2}(H_\varphi B_\varphi - H_r B_r) \quad (6)$$

$$T_{\varphi r} = H_\varphi B_r \quad (7)$$

$$T_{r\varphi} = H_r B_\varphi \quad (8)$$

According to Figure 11:

$$\cos(\mathbf{n}, \mathbf{1}_r) = 1,$$

$$\cos(\mathbf{n}, \mathbf{1}_\varphi) = 0,$$

so statement 4 is

$$\begin{bmatrix} F_r \\ F_\varphi \end{bmatrix} = \oint_s \begin{bmatrix} \frac{1}{2}(H_r B_r - H_\varphi B_\varphi) \\ H_\varphi B_r \end{bmatrix} ds \quad (9)$$

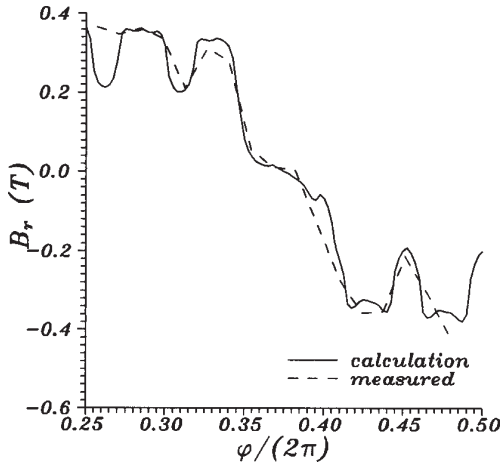

Fig. 9. Zoom of flux density *r*-component in the air-gap of the machine at no-load state

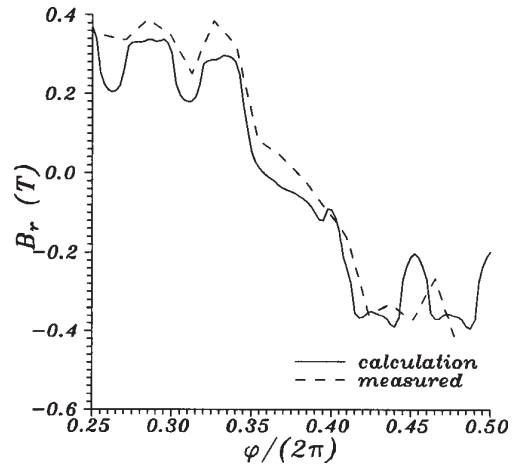

Fig. 10. Zoom of flux density *r*-component in the air-gap of the machine at rated-load state

Tangential and radial component of stress are presented in Figure 12 and 14 (no-load state) and in Figure 13 and 15 (rated load state).

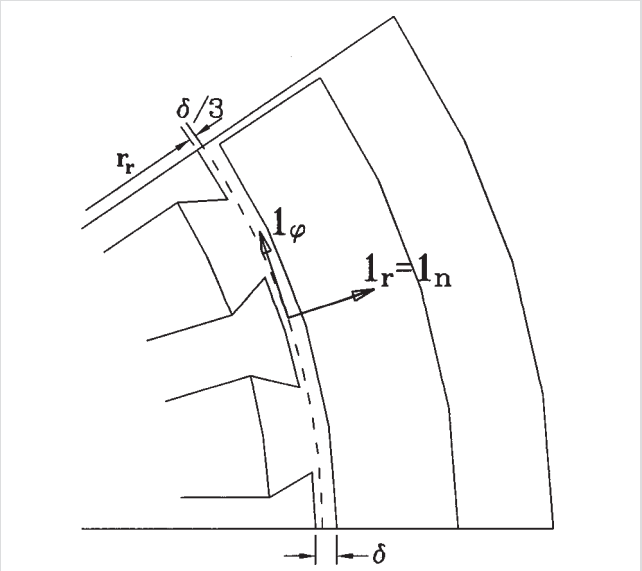

Fig. 11. Integral surface at stress

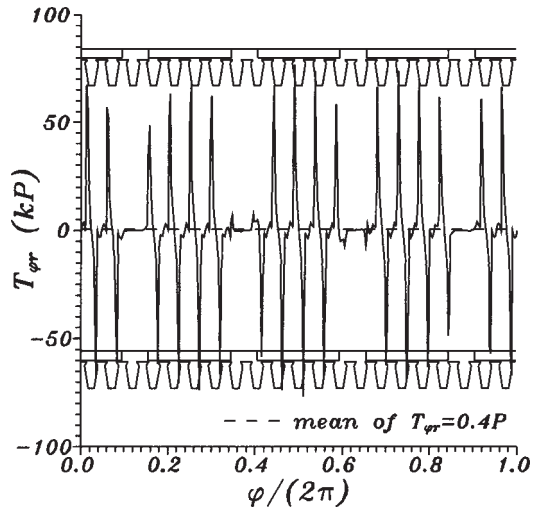

Fig. 12. Stress φ-component of the stator surface of the machine at no-load state

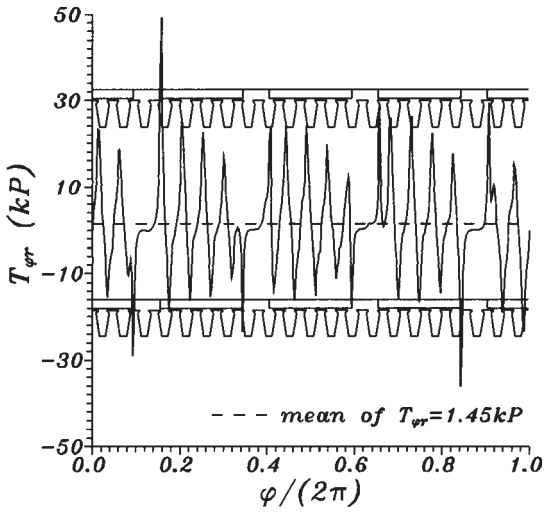

Fig. 13. Stress φ-component of the stator surface of the machine at rated-load state

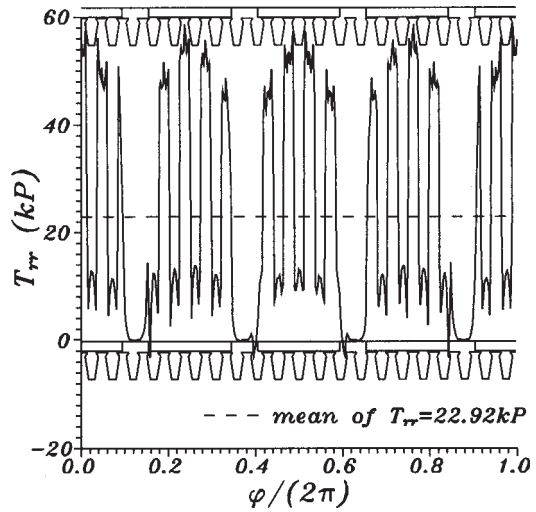

Fig. 14. Stress *r*-component of the stator surface of the machine at no-load state

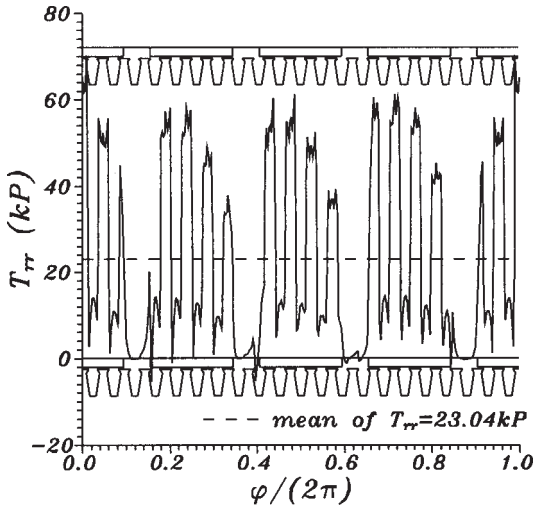

Fig. 15. Stress *r*-component of the stator surface of the machine at rated-load state

4. CONCLUSION

The presented model could be successfully applied for the simulation of steady-state permanent magnet DC-machine. The comparison of the numerical and measurements results leads to the conclusion that the model is sufficiently accurate in the manufacturing point of view.

References

[1] Dudzikowski L: *Permanent magnet DC motors*. Scientific Papers of the Institute of Electric Machine Systems of the Technical University of Wrocław, vol. 42, No. 10, 1992 (in Polish)

[2] Krasucki F., Szymański Z.: *Effect of permanent magnet parameters on selected electromagnetical and electromechanical parameters of DC permanent magnet traction motor.* Proc. of XII Symposium on Electromagnetic Phenomena in Nonlinear Circuits, 1991, 279–283

[3] Skoczylas J.: *Flux distribution of permanent magnet analysis using finite element method.* Archives of Electrical Engineering, vol. XXIX, No. 2, 1980, 293–300 (in Polish)

[4] Wiak S., Komęza K., Pelikant A.: *Computer aided simulation of field and torque of DC permanent magnet motor.* Proc. of XIII Symposium on Electromagnetic Phenomena in Nonlinear Circuits, 1994, 19–24

[5] Wing M., Gieras J.F.: *Influence of angular displacement of a permanent magnet on the performance of a DC commutator motor.* Proc. of XXIX Symposium on Electrical Machines, 1993, 219–224

[6] Zhu Z.Q., Howe D.: *Instantaneous magnetic field distribution in brushless permanent magnet DC motors.* IEEE Transactions on Magnetics, 1993, vol. 29, No. 1, 124–158

Wpłynęło: 27.12.2004

Andrzej MATRAS

Andrzej Matras ukończył studia na Wydziale Elektrotechniki, Automatyki, Informatyki i Elektroniki Akademii Górniczo-Hutniczej w Krakowie w 1970 roku. Doktor nauk technicznych od 1976. Jest pracownikiem naukowym Katedry Maszyn Elektrycznych tej Uczelni.

Główny obszar zainteresowań to maszyny elektryczne i pole elektromagnetyczne.

e-mail: matras@uci.agh.edu.pl